The Journal of The Textile Institute

ISSN: 0040-5000 (Print) 1754-2340 (Online) Journal homepage: www.tandfonline.com/journals/tjti20

Fully textile striped triboelectric electroactive sensors for motion monitoring

J. Blūms, A. Kataševs, E. Mileika, I. Gorņevs, V. Jurķāns, I. Balgale, I. Baltiņa & A. Okss

To cite this article: J. Blūms, A. Kataševs, E. Mileika, I. Gorņevs, V. Jurķāns, I. Balgale, I. Baltiņa & A. Okss (11 May 2025): Fully textile striped triboelectric electroactive sensors for motion monitoring, The Journal of The Textile Institute, DOI: 10.1080/00405000.2025.2502892

To link to this article: https://doi.org/10.1080/00405000.2025.2502892

THE JOURNAL OF THE TEXTILE INSTITUTE
https://doi.org/10.1080/00405000.2025.2502892

Taylor & Francis
Taylor & Francis Group

RESEARCH ARTICLE

OPEN ACCESS Check for updates

Fully textile striped triboelectric electroactive sensors for motion monitoring

J. Blūms[a], A. Kataševs[b], E. Mileika[c], I. Gorņevs[a], V. Jurķāns[a], I. Balgale[c], I. Baltiņa[c] and A. Okss[c]

[a]Institute of Technical Physics, Riga, Latvia; [b]Institute of Biomedical Engineering and Nanotechnologies, Riga, Latvia; [c]Institute of Architecture and Design, Riga, Latvia

ABSTRACT

This study develops a novel, fully textile-knitted electroactive motion sensor based on the triboelectric effect. The sensor consists of knitted elements with different electroactivity, connected by conductive threads to measure electrical signals. When the wearer moves, charge transfers between clothing parts, inducing electric current pulses between the conductive elements. The pulse shape, amplitude, and length depend on movement speed and pressure. The study used a modified Martindale tester and processes described by the proposed theoretical model. Results show that the induced voltage pulses can reach 1.2 V, depending on contact surface area, pressure, and movement speed. This sensor can be seamlessly integrated into knitwear as a design element without compromising comfort and can be manufactured using commercially available yarn during knitwear production.

ARTICLE HISTORY
Received 28 July 2024
Accepted 30 April 2025

KEYWORDS
smart textiles; knitted structures; electroactive sensors; triboelectric effect; jersey fabric

1. Introduction

Over the last two decades, wearable electronic devices integrated into garments have been widely used for monitoring vital physiological and biomechanical signals related to human health and dynamic posture. Nowadays, wearable devices have fostered an attractive lifestyle for people, with numerous commercial products already available. It is also essential for telemedicine and patient daily observations to promptly identify and correct abnormal physiological conditions and improper movement postures to prevent potential hazards to human health. Smart devices must be comfortable, easy to use, and seamlessly connected to the body. Thus, many new devices are under development, considering trends in miniaturization, portability, multifunctionality, and flexibility.

Textiles, recognized for their flexibility and comfort, are widely used daily. Among textile fabrics, knitted structures have greatly improved elasticity, enhanced broad strain range, and provided the best fit to complex surfaces (Kwak et al., 2017). Modern computerized knitting machines can integrate special functional yarns into the base fabric to create local areas with specific stitch structures and physical properties (optical, mechanical, electro- and thermoconductive, etc.). Hence, knitting technology is the most preferable for developing and integrating sensing elements to provide "smart" properties to clothing. Many smart textile devices have been developed using knitting technology: knitted washable chest bands for monitoring breathing signals (Raji et al., 2020), smart socks for gait monitoring (Oks et al., 2017), electrode systems for ECG and EMG monitoring (Alizadeh-Meghrazi et al., 2022; Nigusse et al., 2021), and more. Due to the high deformability of knitted structures, knitted sensors can detect even tiny movements, which have been used in smart shirts and trousers for movement retraining (Eizentals et al., 2020) and post-stroke rehabilitation (Kozirevs et al., 2023).

A common trait of all the aforementioned sensors is the necessity of electrical power to provide data; hence, more sensors mean higher power consumption. Power sources, typically batteries, are bulky and much stiffer than basic garments even in their flexible versions. Therefore, power sources are poorly integrated into knitted structures, compromising the preferability and comfort of knitwear (Zhang et al., 2016). To overcome this problem, biomechanical energy harvesting and its conversion into electrical energy using the Seebeck effect (Nozariasbmarz et al., 2020), electromagnetic induction (Gorņevs et al., 2023), triboelectric nanogenerators (TENG) (Jurķāns et al., 2018; Liu et al., 2019; Pu et al., 2016; Zhang et al., 2016), as well as different wearable machines (Kuang et al., 2017) have been proposed.

With advantages such as being environmentally friendly, easy to manufacture, low-cost, and using a wide range of materials, TENG is better suited than other methods for powering smart wearable electronics by transforming the wearer's motion energy into electric energy. However, the most effective TENGs require special materials and specific designs incompatible with industrial knitting technologies (Dong et al., 2017; Seung et al., 2015; Zhao et al., 2016). Most developed textile-based TENGs, including knitted TENGs (t-TENGs), incorporate specially designed core-spun

CONTACT J. Blūms Juris.Blums@rtu.lv Institute of Technical Physics, Riga Technical University, 6A Kipsalas str., Riga, LV1658, Latvia.
Supplemental data for this article can be accessed online at https://doi.org/10.1080/00405000.2025.2502892.

or core-sheath wires and yarns, which have essential thickness and relatively low flexibility compared to traditional yarns (Fan et al., 2020; Pu et al., 2016; Yu et al., 2017). Thus, they are unsuitable for thin knitted fabrics for sports apparel, underwear, or casual garments (except thick knitwear knitted on low gauge knitting machines). Several known solutions (Dong et al., 2020; Kwak et al., 2017) use commercially available traditional yarns such as cotton, polyamide (PA), polyester (PES), and some electroconductive yarns, such as silver-coated polyamide. Still, they demonstrate a relatively low ability to generate electrical energy based on triboelectricity. On the other hand, their dependence on the external impact can be used to determine and characterize the physical influence. Thus, instead of harvesting energy from t-TENG deformation, the generated pulses are used as informative signals of the deformation of the t-TENG structure or its elements. However, when designing t-TENGs with structures that are very sensitive to applied force, deformation and structural topology variations become important. This approach has been demonstrated in previous studies (Dong et al., 2020; Kwak et al., 2017). Both developed t-TENGs were designed as multilayered membrane structures in which knitted triboelectric layers were connected/separated under periodic tension or compression. T-TENGs were integrated into apparel by stitching processes and using intarsia knitting. The latter ensures the fabrication of t-TENG and its seamless integration into knitwear during manufacturing. Proposed t-TENGs have demonstrated the possibility of creating fully knitted textile energy generators and using them as self-powered pressure sensors. However, due to the increased thickness of their structures, these solutions can compromise the aesthetic and wearing comfort of the apparel. Additionally, these t-TENGs only work properly with significant deformation of their structure. In (Somkuwar & Kumar, 2023), the efficacy of rib-knitted and woven TENG-based sensors fabricated from commercially available yarns was studied. Nylon and cotton yarns were used for the positive triboelectric layer, while polypropylene (PP) and nylon yarns were employed for the negative triboelectric layer. Due to their higher surface roughness compared to woven fabrics, the study demonstrated that knitted structures provide significant increases in output voltage, current, and power.

Several recent studies have highlighted effective applications of self-powered sensors (Liu et al., 2018; Saville, 1999; Somkuwar et al., 2024; Somkuwar & Kumar, 2023; Wang et al., 2023; Zhou et al., 2020). In particular (Somkuwar et al., 2024), describes the development of a low-cost, self-powered sock-insole system for gait monitoring, utilizing embroidery techniques for sensor fabrication. A key advantage of this approach is its reliance on commercially available polymer fabrics and socks.

In (Somkuwar et al., 2024), several novel t-TENG structures using nylon-PP yarns as a triboelectric pair for self-powered sensors were proposed. The plated and ridge structures demonstrated the highest peak power densities and provided the strongest signal outputs. These structures have relatively low thickness and good air permeability and can be integrated into garments using commercial knitting machines. However, the authors recommended using monofilament copper yarn to ensure signal output. This solution presents challenges for scalable knitting processes due to copper yarn's low flexibility and relatively high brittleness under bending stress.

In contrast, other solutions (Saville, 1999; Somkuwar & Kumar, 2023; Wang et al., 2023; Zhou et al., 2020) primarily rely on specially designed yarns and relatively thick, multilayered textile-based structures or combinations with polymer films, similar to the t-TENGs discussed above. Furthermore, most of these sensors operate in contact-separation mode, making them less suitable for monitoring reciprocating motion.

Triboelectric nanogenerator-based sensors can be called "self-powered sensors" because they can convert mechanical energy from their environment into electrical signals, enabling them to operate without external power sources. However, the authors of this paper propose that the term "electroactive sensors" may be more appropriate, as these sensors primarily generate electrical signals in response to mechanical stimuli but do not supply power to themselves or external devices. Therefore, the term "electroactive sensors" will be used in the following discussion.

This research focuses on developing and characterizing a novel, electroactive sensor for monitoring reciprocated motions where electrodes for capturing the generated voltage pulses are knitted in a single textile layer and fabricated using commercially available yarns and traditional knitting techniques. The sensor leverages modified sliding and free-standing modes of the t-TENG (Wang et al., 2023), resulting in an amplified signal. A standardized textile testing setup is utilized to assess the generative properties of the proposed knitted structure. The principle of operation has been proposed and original phenomenological and corresponding mathematical models to describe charge transfer and voltage pulse generation are developed.

2. Materials and methods

The proposed electroactive sensor consists of two parts: a fixed part and a moving part, as illustrated in Figure 1(a), Fixed part consists of dielectric (A, B) and electroconductive (E) strips sequentially knitted in a specific order (A-E-B-E-A). According to the triboelectric series, dielectrics A and B have different charge affinities (Zhou et al., 2020). Dielectric C, which makes up the moving part of the sensor, has a charge affinity between materials A and B. Material selection ensures that when body C is in contact with A, it becomes positively or negatively charged. When it contacts with B, it acquires an opposite charge.

2.1. Fabrication of sensor structure

Knitting technology was used to fabricate the sensor's stationary part, which was knitted using a flatbed knitting machine with a gauge 6 in plain jersey, forming strips of three different materials (Figure 1). The dielectric strips A and B were knitted using polyester yarn (4-ply, resulting in

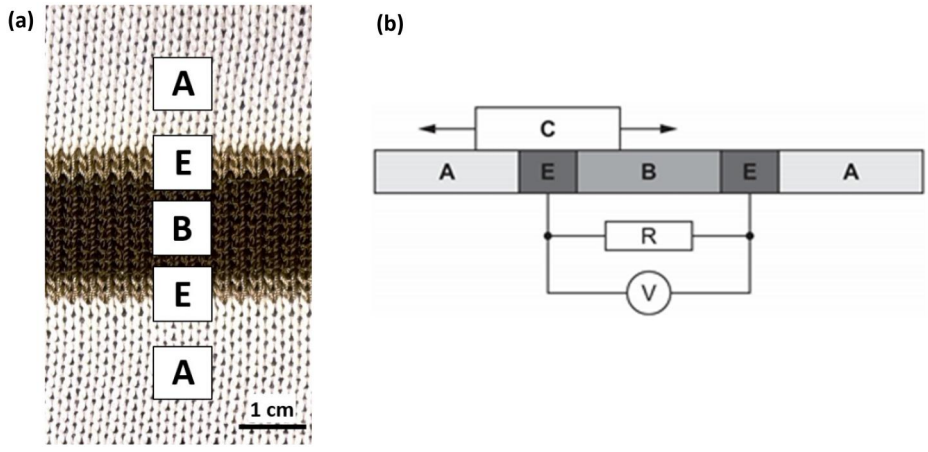

Figure 1. The photo of the knitted structure (a) and the schematic structure of the knitted sensor with the measuring circuit (b): A, B – dielectric knitted stripes, E – electroconductive knitted stripes, C – moving dielectric material, R – load resistance, V – voltage measuring module.

a linear density of 2200tex, 14 twists per cm) and polyamide yarn (2-ply, resulting in a linear density of 2000 dtex, 6 twists per cm); the conductive strips E were made of silver-coated polyamide yarn (Shieldex 235/36 4-ply, result linear density for silverized yarn 130 tex, 18 twists per cm). In the knitting of the conductive strip, two silver-coated yarns are used together to ensure the necessary density of the knit—the stitch density of knitted samples: 4 wales per cm, 6 courses per cm.

The samples measuring 140 × 140 mm were fabricated, as shown in Figure 1b. Each sample featured a central polyamide strip (B) with a fixed width of 17 mm (10 rows). The widths of the conductive (E) and polyester strips (A) were varied to assess their impact on the overall performance.Specifically, samples were knitted with conductive stripes of 1, 3, 5, 7, and 8 courses, corresponding to widths ranging from 2 to 15 mm. The widths of the polyester strips (A) were adjusted accordingly to maintain the total width of each sample at 140 mm.

Two types of industrially produced fabrics were used for the moving element C. Both fabrics were 100% cotton, but one was knitted and the other woven. A jersey fabric weighing 160 g/m^2 and knitted from a yarn with a linear density of 200 tex, stitch density of 16 wales per cm, and 19 courses per cm were used for knitted element C. For a woven type of element C, the fabric parameters are plain weave fabric weighing 130 g/m^2, the number of threads per unit length was 20 ends per cm, and 26 picks per cm.

2.2. Experimental procedure

A Martindale tester (SDL ATLAS M235) was adapted to determine the induced charges when the moving dielectric material C passes over the knitted structure in a back-and-forth direction (Figure 2) [supplementary video 1].

The Martindale tester is a standard testing instrument that determines various fabrics and materials' abrasion and pilling resistance (Saville, 1999). The Martindale testing apparatus consists of a base plate carrying the abrading tables and the drive mechanism, which causes the specimen holder guide plate to move in one direction or trace a Lissajous figure to

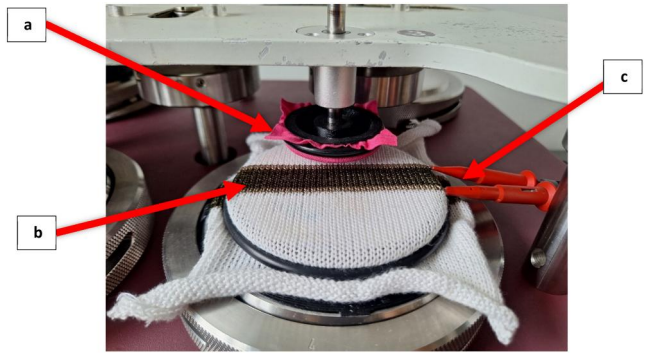

Figure 2. Position of the knitted structure on the martindale tester table: a – moving sample holder (C on Figure 1), b – fixed knitted sensor, c – measuring leads on conductive strips (E on Figure 1).

simulate even wear (Textiles, 1998). Customized dielectric circular specimen holders were used to measure induced charge. During testing, specimens can be subjected to different loads, speeds, directions of movement, and number of continuously performed rubs, which makes it possible to measure the dependence of the induced charge on various parameters. The tests were performed on the face side of the knitted fabric in the direction of the wales. The movable sample holder (dielectric C in Figure 1) moves along the knitted sample in a back-and-forth direction, traveling 6 cm in one direction. The moving sample holder of the tester was modified by reducing its diameter to 1 cm, which coincides with the width of the B band of the samples.

2.3. Measuring circuit

Induced voltage pulses (Figure 3) were registered by USB oscilloscope PicoScope 5444D in conjunction with the high impedance preamplifier of the Keithley 6514 electrometer. For simplicity, schematics will only display a single voltmeter V. The presented measurements are obtained on a matched electric load, experimentally determined for each specimen, and set using thick-film high-voltage resistors. Most of the generated energy is in a frequency range below

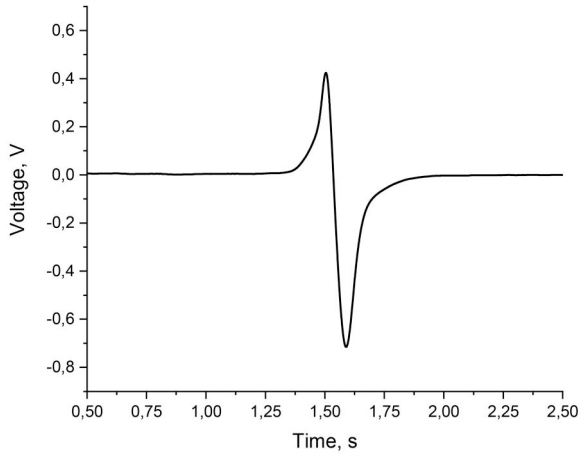

Figure 3. The voltage pulse induced in a load resistance by one motion of the sample holder (C in Figure 1, a in Figure 2) over a striped structure.

50 Hz. Therefore, the capacitive part of the input impedance can be neglected.

Measured voltage waveforms were used to calculate the induced charge (Equation (1)) and generated energy per pulse (Equation (2)).

$$Q = \int \frac{u(t)}{R} dt; \tag{1}$$

$$W = \int \frac{u(t)^2}{R} dt \tag{2}$$

where $u(t)$—the instantaneous value of generated voltage, R resistance of the load resistor.

3. Results and discussion

3.1. Experimental results

The first experiment stage used knitted moving elements (C in Figure 1). Measurements were made for the cases of its movement along courses and wales. Both cases showed similarity in signal shape and studied dependencies, but some differences in absolute values have been obtained (Figure 4).

As presented in Figure 4, such difference can be explained by anisotropy of knitted structure in course and wale directions. To exclude the influence of anisotropy of the structure of the moving element on the sensor signal, the knitted moving element was changed by the woven one with low anisotropy in warp and weft directions. Thus, further results reported were obtained with the woven moving element.

The pulses induced during sliding of material C at different pressures are shown in Figure 5. As the pressure increases, the amplitude of the induced voltage pulses also increases, which is explained by the increase in the contact surface and the increase in friction as the pressure increases. The pressure dependence of the corresponding induced charge and generated energy is shown in Figure 6. The amount of energy generated during one movement also depends on the movement speed of the sample holder C.

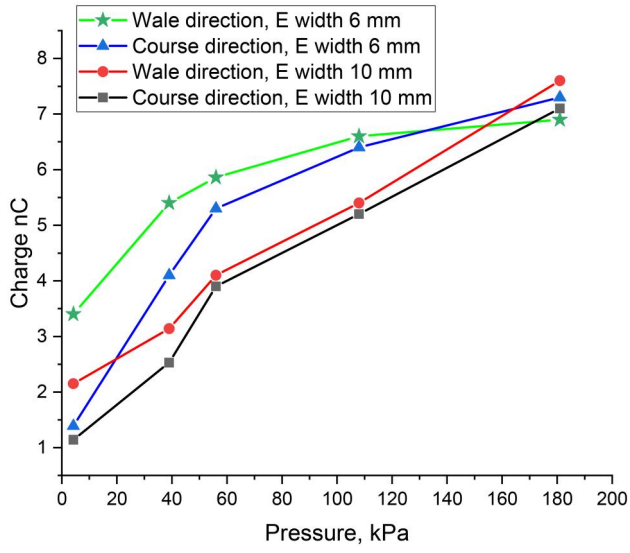

Figure 4. The dependence of the induced charge on the direction of the sample holder motion (wales and courses) and the width of conductions stripes (E width).

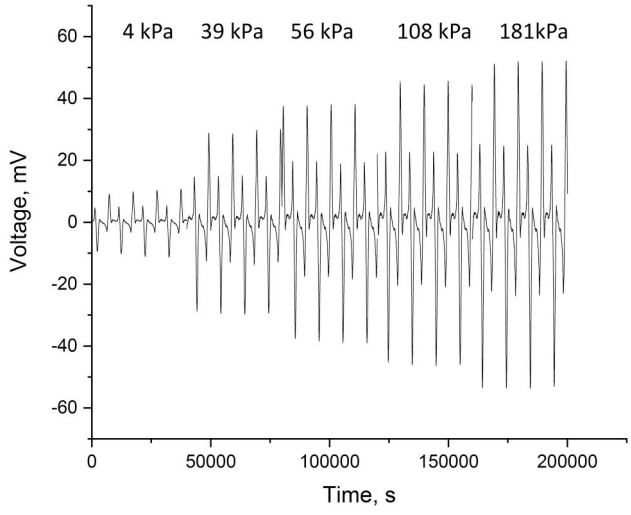

Figure 5. The shape and amplitude of the generated voltage pulses as a function of the pressure between the sensor and the sample holder C.

Figure 7 shows this dependence for different sensors with different sizes of E stripe.

3.2. Principle of operation of proposed electroactive sensors

The electroactive sensor's operation is based on the triboelectric effect to charge the moving material C when sliding over non-conductive materials A and B, as presented in Figure 8. Material selection for bands A and B ensures that when dielectric C is in contact with A (Figure 8(a)), it becomes positively or negatively charged. When in contact with B (Figure 8(c)), it acquires an opposite charge. Encountering the conductive stripes E (Figure 8(b) and (d)), charged material C induces the displacement of the charge through the load resistance R, which is detected by the voltmeter V. Due to opposite charging polarity, the pulses

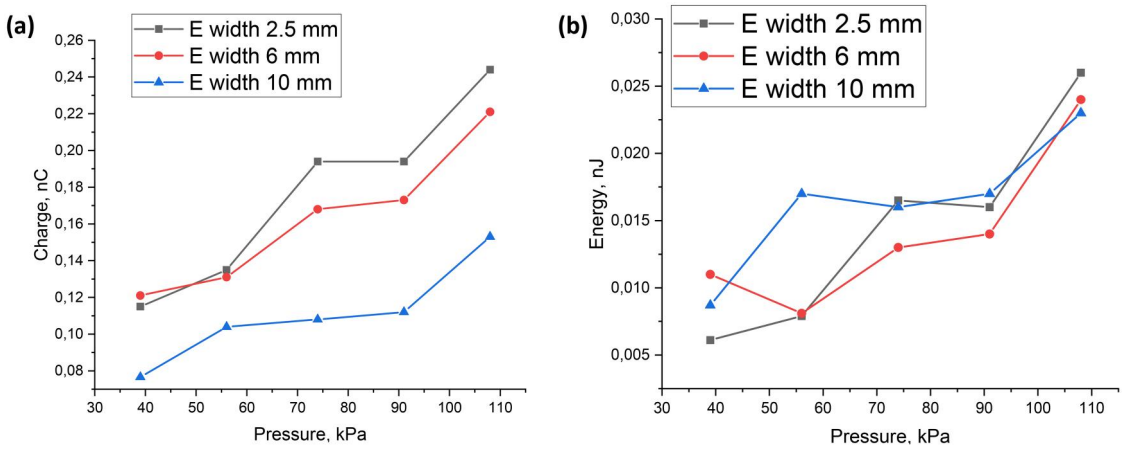

Figure 6. Dependence of the induced charge (a) and the generated energy (b) per movement on the pressure of the sample holder.

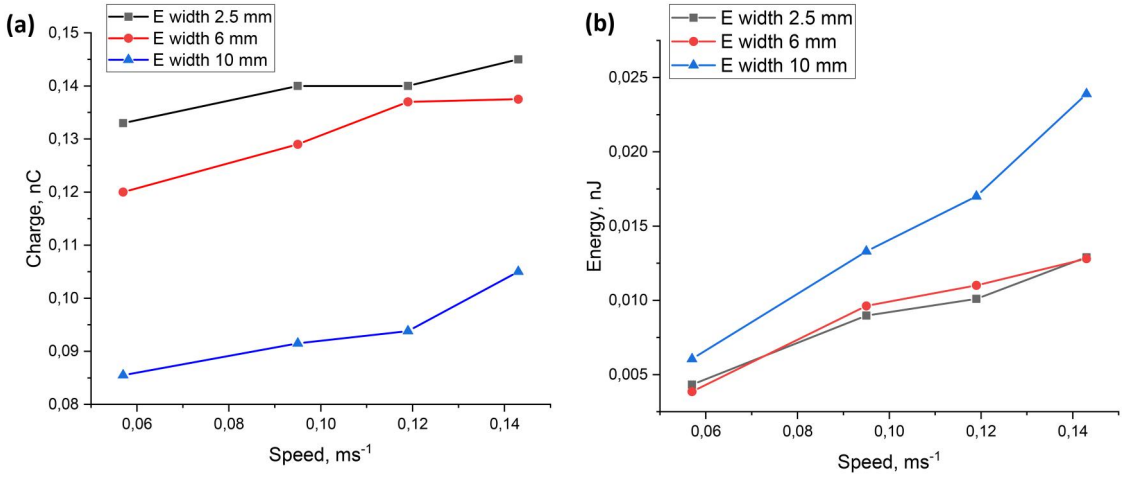

Figure 7. Dependence of the induced charge (a) and the generated energy (b) per movement on the speed of the sample holder.

generated in electrodes *E* are with one polarity and amplify each other.

When the direction of the sample holder C movement changes, the charging and discharge processes repeat themselves, creating an electric pulse of the same shape.

3.3. The theoretical model and simulation of sensor behavior

The following phenomenological model is proposed to describe voltage pulse generation by process explained in Section 3.2. Moving over the dielectric area A, the applicator gains positive surface charge q_{ext} due to charge exchange between cotton and polyester (A in Figure 8(a)). In the model, the surface charge is characterized by the surface charge density σ_A. The total charge *next, accumulated by the dielectric on the sample holder C during contact with dielectric A, induces electrostatic potential* φ_{ext} *in the first zone E electrode (leftmost zone E in* Figure 8). The induced potential attracts electric charge, flowing from the ground through the load resistor (Figure 8(b)). This current charges the electrode E with induced charge q_{ext} until the induced potential equalizes the external potential φ_{ext} (Figure 9).

During the motion over area B, the sample holder's C surface charge density changes to σ_B due to charge exchange

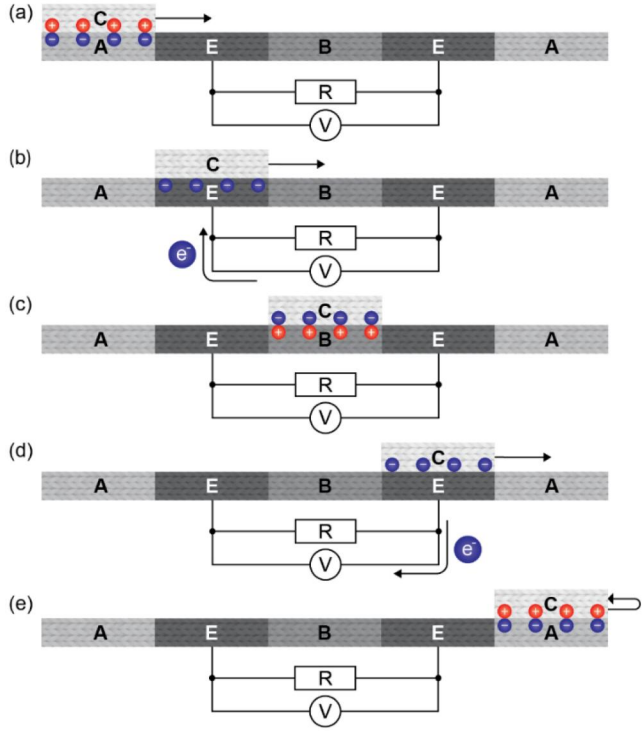

Figure 8. Charge transfer scheme during the sample holder motion through the knitted sensor.

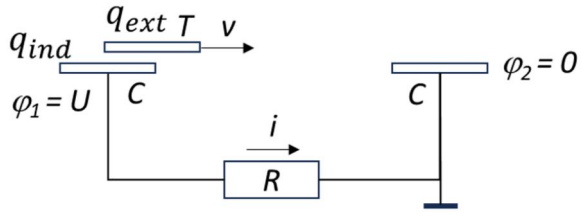

Figure 9. Load equivalent circuit.

between cotton and polyamide (Figure 8(c)), but this charge still induces the potential over the first zone E electrode. Moving over the second zone E electrode, the applicator discharges to the ground (Figure 8(d)) and recharges while moving over the second zone A (Figure 8(e)).

The definition of the surface charge density *σand its variation with time is the most critical part of the model, as it is related to the charge exchange mechanism* between the zone material and the applicator. As the first approach, the simplified model uses a set of assumptions. First, the charge exchange between the textile on the sample holder C and the dielectric surface of polyester (zone A) or polyamide (zone B) is considered instant, as the mechanical motion of the applicator is considerably slower than the typical rate of electron exchange processes. I.e., each surface element of the applicator that contacts either material A or B instantly gains a triboelectric surface charge equal to either σ_A or σ_B, correspondingly. Second, the model ignores the potential discharge of the applicator through resistor R to the ground because of the high value of the R (approx. 1GΩ).

Within such assumptions, the net potential of electrode φ_1, which is equal to the measured voltage U over the load resistor, is a superposition of the external potential φ_{ext}, induced by the charged material on holder C and induced potential φ_{ext}, that appears due to the accumulation of induced charge q_{ext} on the electrode:

$$\varphi_1 = \varphi_{ext} - \varphi_{ind} \tag{3}$$

the minus sign already accounts for the negative polarity of the electrode charge caused by the positively charged applicator. The second electrode is grounded, and its potential is zero. Therefore, potential φ_1 equals the voltage U, measured across resistance R. The current through the resistor is

$$i = \frac{1}{R}(\varphi_{ext} - \varphi_{ind}) \tag{4}$$

When the capacitance of electrode C is introduced, the induced potential of φ_{ind} can be described as $\varphi_{ind} = q_{ind}/C$. Capacitance C will be one of the model's tuning parameters. Taking the derivation of Equation (4) by time and noting that $dq_{ind}/dt = i$, one gets

$$\frac{di}{dt} = \frac{1}{R}\left(\frac{d\varphi_{ext}}{dt} - \frac{i}{C}\right) \tag{5}$$

Multiplying by R and noting $U = iR$, one can get the principal first-order ODE equation of the model:

$$\frac{dU}{dt} = \frac{d\varphi_{ext}}{dt} - \frac{1}{RC}U \tag{6}$$

with the initial condition $u(t = 0) = 0$;

The external induced potential is given by:

$$\varphi_{ext} = \int_S k\frac{\sigma(z,t)}{d(z,t)}dS \tag{7}$$

where $k = 8.99 \times 10^9$ N m^2 C^{-2} is the electric constant, but functions $\sigma(z, t)$ and $d(z, t)$ represent the surface charge density of the applicator's element and its distance to the conductive electrode. Here z is a coordinate on the applicator surface. Note that the definition of $d(z, t)$ includes tuning parameter h, which is the effective minimal distance between the applicator and electrode. The h could be interpreted, for example, as a distance between the plates of a plain capacitor, equivalent to the capacitor, formed by the applicator and conductive electrode. Because the sample holder C is moving, both parameters, σ and d, are functions of coordinates z and time t.

With all assumptions made, the function $\sigma(z, t)$ has the following values:

$$\sigma(z,t) = \begin{cases} \sigma_A & \textit{applicator in the first zone A or the first zone E} \\ \sigma_B & \textit{applicator in zone B} \\ 0 & \textit{applicator in the second zone E(grounded)} \\ \sigma_A & \textit{applicator in the second zone A} \end{cases} \tag{8}$$

The detailed equations of the proposed model, as well as the calculation algorithm, are provided in the Appendix.

The model has several unknown parameters that depend on the physical properties of the materials and the setup. So far, these parameters can be tuned by using experimental results:

1. h - effective minimal distance between applicator and electrode,
2. C – effective capacitance of the first conductive electrode,
3. σ_A - applicator's charge density after charging in zone A,
4. $\sigma_B - \sigma_A$ - applicator's charge density after charging in zone B.

The model parameters were adjusted using the least square method to match the experimental waveform. According to the model, the shapes of predicted pulses are generally in a fair qualitative coincidence with the experimentally observed ones (Figure 10), especially for narrow conductive lines less than 6 mm in width (Figure 10(a, b, c)). Nevertheless, the quantitative values of the surface charge are in poor agreement with both literature data and estimation from the experimental results. The literature data proposes values of the typical surface charge densities in the range of 1 pC cm^{-2}—8 nC cm^{-2} for polyamide, polyester and cotton (Liu et al., 2018; 2022), that exceed model parameters too.

At the same time, the model reasonably prognoses the effect of applicator velocity and applicator applied pressure. With the increase in applicator velocity, the total generated power increased both in the experiment (Figure 7) and in the model (Figure 11).

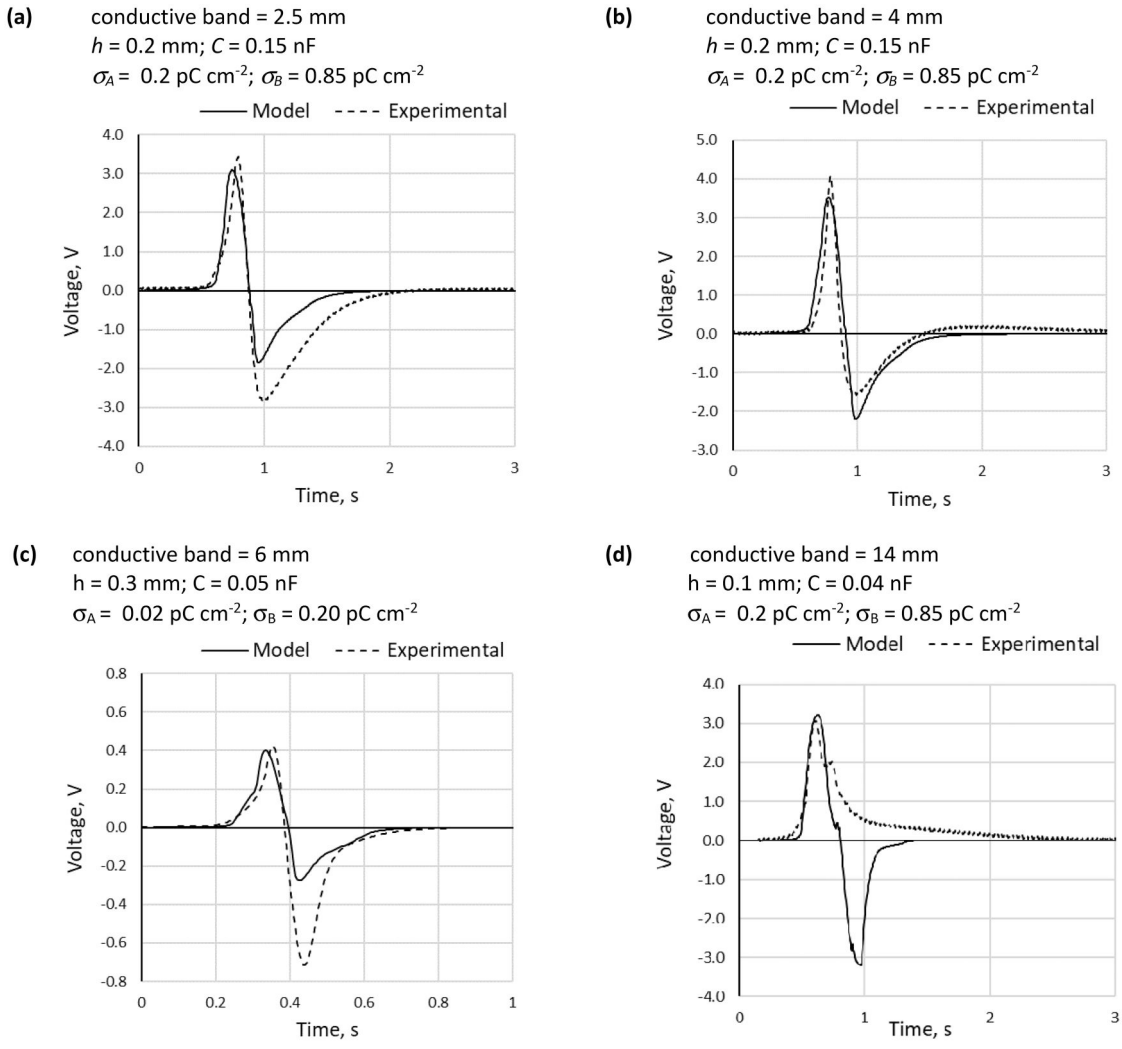

Figure 10. Results of the voltage waveform modelling and experiment with different width of conductive band.

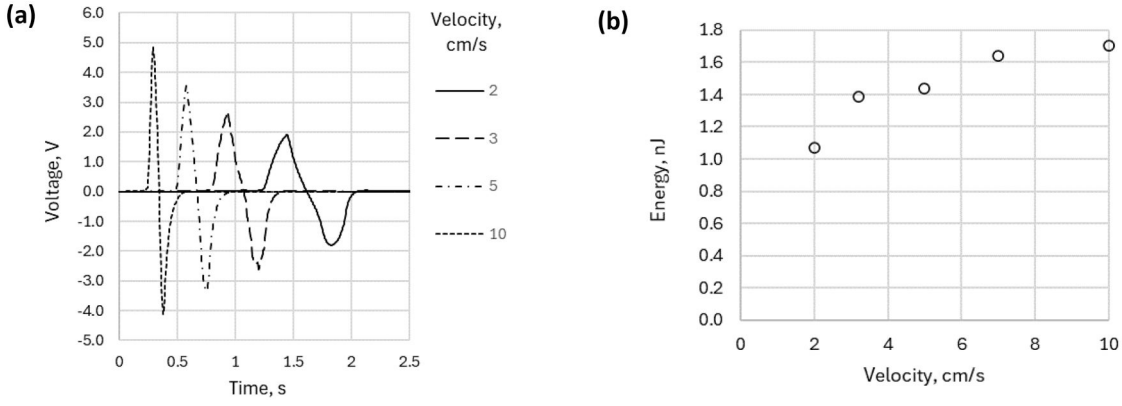

Figure 11. Model—predicted effect of the applicator velocity on the generated waveform (a) and energy (b).

The applicator pressure is not included in the proposed model. Nevertheless, increased pressure could decrease the effective gap h between the applicator and the knitted structure. From this point of view, the decreased value of the gap could represent applied pressure, which in turn increases total generated energy (Figure 12(b)) in a model in a similar way to how the increase in pressure raises generated energy in the experiment (Figure 6(b)).

The modeling results demonstrate a quantitatively adequate description of the voltage waveform. This may be an argument to claim that the electrical induction, which the model is based upon, plays a major role in the sensor voltage generation. Nevertheless, the numerical discrepancies between the experimental and modeled waveforms insist on consideration of other mechanisms. One of the most important deviations from the expected results is the sign of the

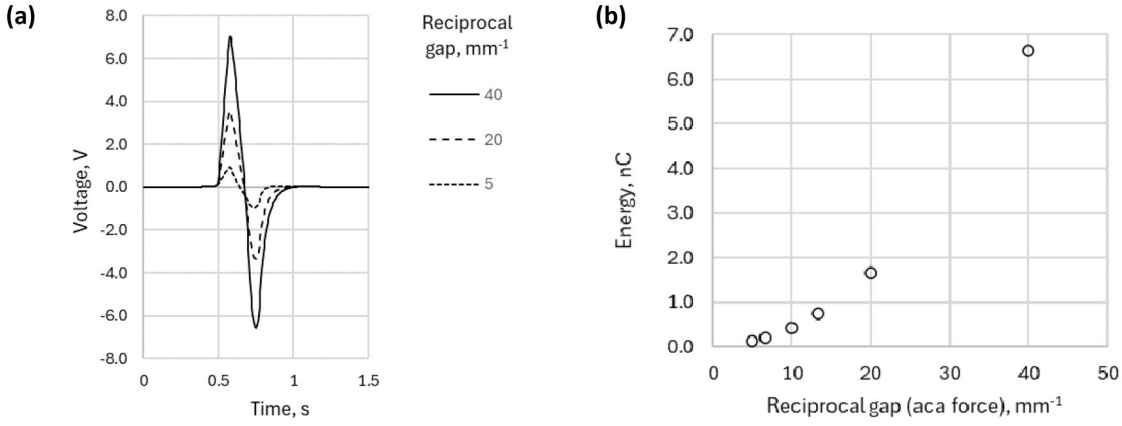

Figure 12. Model-predicted effect of the reciprocal gap value between the applicator and knitted structure on generated waveform (a) and energy (b).

generated charge. While literature data (Liu et al., 2018; 2022) suggests that cotton should possess a positive charge in contact with PES but negative in contact with PA, the model gives good agreement when cotton is charged positively in both PES and PA areas. Although the possible explanation could be the experimental conditions that in the present research differed from (Liu et al., 2018; 2022), the future model should include other mechanisms of charge exchange between the applicator and dielectric materials and consider the discharge of the applicator *via* conductive areas. The discharge can play a more important role for sensors with wide conductive bands, as the applicator remains in contact with the conductor for longer periods, and there is more time for discharge to occur.

4. Integration of sensors in clothing

A prototype of a smart vest was created to demonstrate the functionality of the developed electroactive sensors in a wearable context (Figure 13, supplementary video 2). This vest incorporates sensor zones on both sides, each containing an array of stationary parts of three two electroactive sensors. The prototype was knitted using a hand-flatbed knitting machine with a gauge 6, employing cotton yarn as the base material.

The sensor zones on the sides of the vest are formed by continuously knitted polyester (A) and polyamide (B) stripes, with electrically conductive yarns (E) integrated at specific sensor locations using the intarsia technique. This approach ensures a seamless incorporation of the sensing zones into the base knitted structure.

To ensure proper tension and correct positioning of the sensors, the vest prototype includes adjustable fasteners on its back. The moving component of the sensors was represented by the sleeves of a cotton shirt (C in Figure 13), which was worn beneath the vest prototype. As shown in the supplementary video, the motion of these sleeves, driven by the wearer's arm movements, activated the sensors. The knitted fabric forms the prototype's base and is placed perpendicular to the knitting direction, ensuring the same knitting direction used in the experiments with the samples.

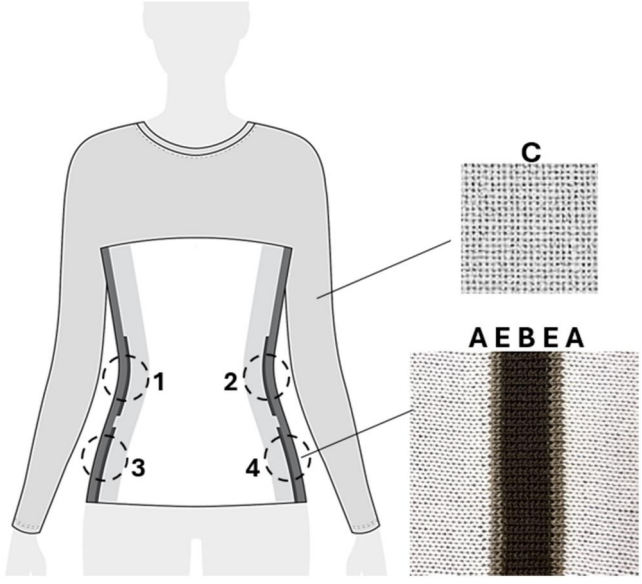

Figure 13. Illustration of sensors placement and structure in a prototype: a knitted vest with fixed sensor zones on both sides (1–4), formed by strips of polyester (a), polyamide (B), electroconductive (E) yarns, and a moving sensor part, formed by cotton (C) shirt sleeves.

The sensors located in this way can monitor the relative movement of the hands along the sides of the body, thereby making it possible to compare the amplitudes of the generated signals and their changes due to changes in the type of movement and posture, which is the content of a separate study. This study aims to study the response of sensors to external effects, so all tests are performed at the laboratory under controlled conditions: fixed and constant pressures and speeds of movement.

The sensor's novelty lies in its banded structure, comprising materials with varying electroactivity (affinity), which are strategically arranged to maximize the generated electrical signal by reloading the upper material to the opposite polarity when moving between electrodes, allowing for more flexible designs. The structure and placement of the system for recording and processing generated electrical signals will depend on the number of sensors, their dimensions, and the type of clothing.

5. Conclusion

A novel, 100% textile body motion sensor has been developed, leveraging knitting technology to integrate into clothing seamlessly. The sensors are fabricated using traditional, commercially available yarns such as cotton, polyamide, and polyester, ensuring a simple and cost-effective design. This design allows easy incorporation into clothing during production, using techniques like intarsia knitting without compromising wearer comfort. The created sensor geometry ensures the generation of electrical impulses of equal polarity in knitted electrodes, reinforcing each other (constructive overlapping).

The fully textile electroactive structures exhibit sensitivity to various movement parameters, including pressure, speed, and structural changes like stripe width, making them suitable for use as movement sensors that are an integral part of clothing. These sensors do not require external power to provide the signal, potentially lessening the measurement circuit's overall power consumption. In the research process, a clothing prototype with knitted sensors has been created and its practical usability for recognizing various types of hand movements has been shown.

A phenomenological electrostatic model has been developed to describe the sensor's behavior, providing a quantitatively accurate description of the voltage waveform. While it suggests that electrical induction plays a major role in voltage pulse generation, discrepancies between experimental and modeled waveforms suggest that other mechanisms, such as charge exchange, may also be involved, particularly in sensors with wide conductive bands.

Disclosure statement

The authors report that there are no competing interests to declare.

Funding

This work was supported by the Latvian Council of Science under Grant Nr. lzp-2022/1-0290, "Development of knitted self-generating sensors: combining physics and knitting technology".

ORCID

J. Blūms http://orcid.org/0000-0002-7087-6062

References

Alizadeh-Meghrazi, M., Sidhu, G., Jain, S., Stone, M., Eskandarian, L., Toossi, A., & Popovic, M. R. (2022). A mass-producible washable smart garment with embedded textile emg electrodes for control of myoelectric prostheses: a pilot study. *Sensors*, *22*(2), 666. https://doi.org/10.3390/s22020666

Dong, K., Wang, Y.-C., Deng, J., Dai, Y., Zhang, S. L., Zou, H., Gu, B., Sun, B., & Wang, Z. L. (2017). A highly stretchable and washable all-yarn-based self-charging knitting power textile composed of fiber triboelectric nanogenerators and supercapacitors. *ACS Nano*, *11*(9), 9490–9499. https://doi.org/10.1021/acsnano.7b05317

Dong, S., Xu, F., Sheng, Y., Guo, Z., Pu, X., & Liu, Y. (2020). Seamlessly knitted stretchable comfortable textile triboelectric nanogenerators for E-textile power sources. *Nano Energy*, *78*, 105327. https://doi.org/10.1016/j.nanoen.2020.105327

Eizentals, P., Katashev, A., Oks, A., & Semjonova, G. (2020). Smart shirt system for compensatory movement retraining assistance: Feasibility study. *Health and Technology*, *10*(4), 861–874. https://doi.org/10.1007/s12553-020-00420-x

Fan, W., He, Q., Meng, K., Tan, X., Zhou, Z., Zhang, G., Yang, J., & Wang, Z. L. (2020). Machine-knitted washable sensor array textile for precise epidermal physiological signal monitoring. *Science Advances*, *6*(11), eaay2840. https://doi.org/10.1126/sciadv.aay2840

Gorņevs, I., Jurķāns, V., & Blūms, J. (2023). Development of wearable multiple source energy-harvesting system for smart clothing. *IEEE Access*, *11*, 100284–100294. https://doi.org/10.1109/ACCESS.2023.3313559

Jurķāns, V., Blūms, J., & Gorņevs, I. (2018). Harvesting electrical power from body heat using low voltage step-up converters with thermoelectric generators, In *2018 16th Biennial Baltic Electronics Conference (BEC)* (pp. 1–4).

Kozirevs, P., Oks, A., & Katashev, A. (2023). Smart textile in post stroke patient rehabilitation exercises evaluation for lower extremities. in *19th Nordic-Baltic Conference on Biomedical Engineering and Medical Physics*., Y. Dekhtyar and I. Saknite (Eds.), Springer Nature Switzerland. (pp. 94–103).

Kuang, Y., Ruan, T., Chew, Z. J., & Zhu, M. (2017). Energy harvesting during human walking to power a wireless sensor node. *Sensors and Actuators A: Physical*, *254*, 69–77. https://doi.org/10.1016/j.sna.2016.11.035

Kwak, S. S., Kim, H., Seung, W., Kim, J., Hinchet, R., & Kim, S.-W. (2017). Fully stretchable textile triboelectric nanogenerator with knitted fabric structures. *ACS Nano*, *11*(11), 10733–10741. https://doi.org/10.1021/acsnano.7b05203

Liu, W., Wang, Z., Wang, G., Liu, G., Chen, J., Pu, X., Xi, Y., Wang, X., Guo, H., Hu, C., & Wang, Z. L. (2019). Integrated charge excitation triboelectric nanogenerator. *Nature Communications*, *10*(1), 1426. https://doi.org/10.1038/s41467-019-09464-8

Liu, S., Zheng, W., Yang, B., & Tao, X. (2018). Triboelectric charge density of porous and deformable fabrics made from polymer fibers. *Nano Energy*, *53*, 383–390. https://doi.org/10.1016/j.nanoen.2018.08.071

Liu, D., Zhou, L., Cui, S., Gao, Y., Li, S., Zhao, Z., Yi, Z., Zou, H., Fan, Y., Wang, J., & Wang, Z. L. (2022). Standardized measurement of dielectric materials' intrinsic triboelectric charge density through the suppression of air breakdown. *Nature Communications*, *13*(1), 6019. https://doi.org/10.1038/s41467-022-33766-z

Nigusse, A. B., Mengistie, D. A., Malengier, B., Tseghai, G. B., & Langenhove, L. V. (2021). Wearable smart textiles for long-term electrocardiography monitoring—a review. *Sensors (Basel, Switzerland)*, *21*, 4174. https://doi.org/10.3390/s21124174

Nozariasbmarz, A., Collins, H., Dsouza, K., Polash, M. H., Hosseini, M., Hyland, M., Liu, J., Malhotra, A., Ortiz, F. M., Mohaddes, F., Ramesh, V. P., Sargolzaeiaval, Y., Snouwaert, N., Özturk, M. C., & Vashaee, D. (2020). Review of wearable thermoelectric energy harvesting: From body temperature to electronic systems. *Applied Energy*, *258*, 114069. https://doi.org/10.1016/j.apenergy.2019.114069

Oks, A., Katashev, A., Bernans, E., & Abolins, V. (2017). Smart socks system as an equipment to analyze temporal parameters of human gait and running. In *Environment. Technology. Resources. Proceedings of the International Scientific and Practical Conference* (vol. 3, p. 238). https://doi.org/10.17770/etr2017vol3.2622

Pu, X., Li, L., Liu, M., Jiang, C., Du, C., Zhao, Z., Hu, W., & Wang, Z. L. (2016). Wearable self-charging power textile based on flexible yarn supercapacitors and fabric nanogenerators. *Advanced Materials (Deerfield Beach, Fla.)*, *28*(1), 98–105. https://doi.org/10.1002/adma.201504403

Raji, R. K., Miao, X., Zhang, S., Li, Y., Wan, A., & Boakye, A. (2020). Knitted piezoresistive strain sensor performance, impact of conductive area and profile design. *Journal of Industrial Textiles*, *50*(5), 616–634. https://doi.org/10.1177/1528083719837732

Saville, B. P. (1999). Physical Testing of Textiles. In *Woodhead publishing series in textiles*. Elsevier Science. https://books.google.lv/books?id=4-uiAgAAQBAJ

Seung, W., Gupta, M. K., Lee, K. Y., Shin, K.-S., Lee, J.-H., Kim, T. Y., Kim, S., Lin, J., Kim, J. H., & Kim, S.-W. (2015). Nanopatterned textile-based wearable triboelectric nanogenerator. *ACS Nano*, *9*(4), 3501–3509. https://doi.org/10.1021/nn507221f

Somkuwar, V. U., & Kumar, B. (2023). Influence of the fabric topology on the performance of a textile-based triboelectric nanogenerator for self-powered monitoring. *ACS Applied Polymer Materials*, *5*(4), 2323–2335. https://doi.org/10.1021/acsapm.2c01820

Somkuwar, V. U., Maurya, S. K., & Kumar, B. (2024). Highly comfortable and durable single-layer knitted textile-based triboelectric nanogenerator for smart wearable applications. *ACS Applied Polymer Materials*, *6*(1), 407–418. https://doi.org/10.1021/acsapm.3c02087

Textiles. (1998). *Determination of the abrasion resistance of fabrics by the Martindale method*. https://www.iso.org/obp/ui/en/#iso:std:1931:en

Wang, Z. L., Yang, Y., Zhai, J., & Wang, J. (2023). *Handbook of triboelectric nanogenerators*. Springer Nature.

Yu, A., Pu, X., Wen, R., Liu, M., Zhou, T., Zhang, K., Zhang, Y., Zhai, J., Hu, W., & Wang, Z. L. (2017). Core–Shell-yarn-based triboelectric nanogenerator textiles as power cloths. *ACS Nano*, *11*(12), 12764–12771. https://doi.org/10.1021/acsnano.7b07534

Zhang, K., Wang, Z. L., & Yang, Y. (2016). Conductive fabric-based stretchable hybridized nanogenerator for scavenging biomechanical energy. *ACS Nano*, *10*(4), 4728–4734. https://doi.org/10.1021/acsnano.6b01170

Zhao, Z., Yan, C., Liu, Z., Fu, X., Peng, L.-M., Hu, Y., & Zheng, Z. (2016). Machine-washable textile triboelectric nanogenerators for effective human respiratory monitoring through loom weaving of metallic yarns. *Advanced Materials (Deerfield Beach, Fla.)*, *28*(46), 10267–10274. https://doi.org/10.1002/adma.201603679

Zhou, L., Liu, D., Wang, J., & Wang, Z. L. (2020). Triboelectric nanogenerators: Fundamental physics and potential applications. *Friction*, *8*(3), 481–506. https://doi.org/10.1007/s40544-020-0390-3

Appendix

The geometry of the experiment is represented as follow (Figure 14):

The material's A (polyester) dielectric layers (zone A) have a length of l_1, the material's B (polyamide) dielectric layer (zone B) has a length of l_2, the electrodes E, made of conductive threads (zones E) have a length l_0. The cotton applicator of radius r slides over the material bands with velocity V in the direction of the X-axis. The position of the applicator is defined by central point x_0. The dielectric and contact zones are defined by coordinates x_1–x_5. The width w of the material exceeds the diameter of the applicator by 5 to 10 times ($w \gg r$).

The potential φ_{ext}, induced on the electrode by the charged applicator, is calculated as a superposition of potentials induced by infinitesimal elements dS of the applicator surface (Figure 15).

Each applicator's element dS is considered a point charge σdS, located at the distance d from the electrode surface. The model introduces the effective gap h between the applicator and electrode as a model tuning parameter. The d is considered to be the distance between element dS and the closest point of the electrodes: for instance, for the element dS left to the point x_1, the distance d is between the element and the top left corner of the electrodes, but for elements right to the x_1 it will be equal to h (Figure 15). Introducing coordinates Z0Y in the applicator's plane, with axis Z collinear to the axis X and $z = 0$ at the center of the applicator, the applicator-induced potential φ_{ext} becomes:

$$\varphi_{ext} = \int_S k\frac{\sigma}{d}dS = \int_{-r}^{r}\int_{-\sqrt{r^2-z^2}}^{\sqrt{r^2-z^2}} k\frac{\sigma(z,t)}{d(z,t)}dydz = \int_{-r}^{r} 2k\frac{\sigma(z,t)\sqrt{r^2-z^2}}{d(z,t)}dz, \tag{9}$$

where $k = 8.99 \times 10^9$ Nm^2/C^2 is the electric constant. Because applicator is moving, both σ and d are functions on both coordinate z and time t. The distance is defined, considering the x-coordinate of the element dS as $x = x_0 + z = Vt + z$, where V is the velocity of the applicator:

$$d(z,t) = \begin{cases} \sqrt{(x_1 - Vt - z)^2 + h^2} & , \quad Vt + z < x_1 \\ h & , \quad x_1 \le Vt + z < x_2. \\ \sqrt{(Vt + z - x_2)^2 + h^2} & , \quad x_2 \le Vt + z \end{cases} \tag{10}$$

The definition of the function $\sigma(z, t)$ is the most critical part of the model, as it is related to the mechanism of the charge exchange between the material and the applicator. As a first approach, the present research uses the simplified mechanism of charge exchange. When the applicator element dS enters the dielectric surface of polyester (Figure 13, zone A) or polyamide (Figure 13, zone B), it gains a triboelectric surface charge equal to either σ_A or σ_B, correspondingly. Such charge transfer is considered instant, as the mechanical motion of the applicator is considerably slower than the typical rate of electron exchange processes. When the applicator comes in contact with the grounded electrode, it is assumed that its surface charge instantly

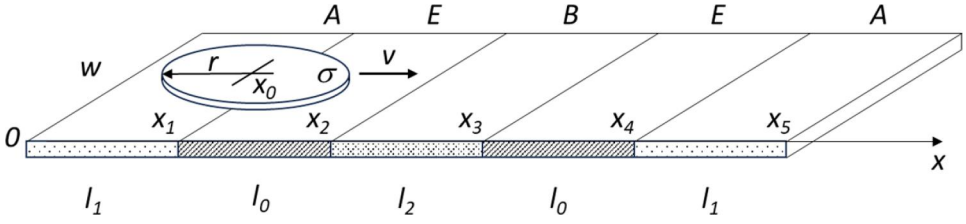

Figure 14. Geometry of the experiment.

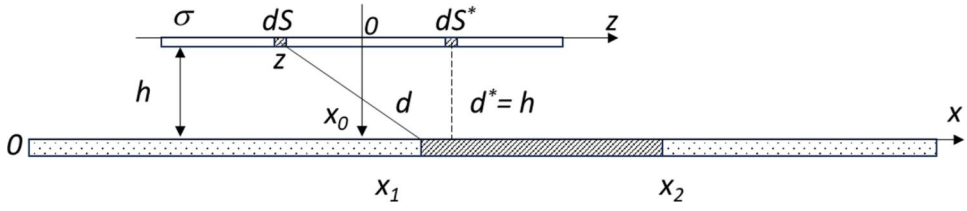

Figure 15. Geometry of the potential induction over the electrode.

becomes zero. For the first approach, the discharge of the element dS during the contact with the first electrode is ignored because the discharge should come *via* a 1GΩ load resistor and *via* contact resistance between electrode and applicator, considered to be high enough. Therefore, the element's surface charge in the first electrode zone is presumed to be equal to σ_A. With all this, $\sigma(z, t)$ becomes:

$$\sigma(z,t) = \begin{cases} \sigma_A & Vt + z < x_2 \\ \sigma_B & x_2 \le Vt + z < x_3 \\ 0 & x_3 < Vt + z < x_4 \\ \sigma_A & x_4 < Vt + z \end{cases} \tag{11}$$

Equations (5–8) form the mathematical model of the voltage induction. As functions $d(z, t)$ and $\sigma(z, t)$ are step-wise, the analytical solution seems unpractical. The system was integrated numerically using the modified Euler method (1st order Runge-Kutta method). The integral in Equation (9) was calculated using the rectangle method. Introducing spatial grid z_j with the step Δz and temporal grid t_i with step Δt, and denoting integral in Equation (9) as F, the calculation task is set as follows:

$$\begin{cases} U_i = 0 \\ \sigma_{i,j} = \sigma_A \end{cases} \tag{12}$$

$$F_0 = \sum_j 2k \frac{\sigma(z_j, 0)\sqrt{r^2 - z_j^2}}{d(z_j, 0)} \Delta z \tag{13}$$

$$F_i = \sum_j 2k \frac{\sigma(z_j, t_i)\sqrt{r^2 - z_j^2}}{d(z_j, t_i)} \Delta z \tag{14}$$

$$\tilde{U}_{i+1} = U_i + \Delta t \left(\frac{F_{i+1} - F_i}{\Delta t} - \frac{1}{RC} U_i \right) \tag{15}$$

$$U_{i+1} = U_i + \frac{\Delta t}{2} \left(\frac{F_{i+1} - F_i}{\Delta t} + \frac{F_{i+2} - F_{i+1}}{\Delta t} - \frac{1}{RC} U_i - \frac{1}{RC} \tilde{U}_{i+1} \right) \tag{16}$$

$$\sigma(z_j, t_i) = \begin{cases} \sigma_A & Vt_i + z_j < x_2 \\ \sigma_B & x_2 \le Vt_i + z_j < x_3 \\ 0 & x_3 < Vt_i + z_j < x_4 \\ \sigma_A & x_4 < Vt_i + z_j \end{cases} \tag{17}$$

$$d(z_j, t_i) = \begin{cases} \sqrt{(x_1 - Vt_i - z_j)^2 + h^2} & , \quad Vt_i + z_j < x_1 \\ h & , \quad x_1 \le Vt_i + z_j < x_2 \\ \sqrt{(Vt_i + z_j - x_2)^2 + h^2} & , \quad x_2 \le Vt_i + z_j \end{cases} \tag{18}$$

For the proposed model, values r, x_1—x_5, V, and R are the experiment's parameters, but parameters h, C, σ_A, and σ_B are the tuning parameters of the model. The model is tuned to obtain solutions close to the experimental voltage waveform.